Determination of principal characteristics of turbulent swirling flow along annuli: part 4: an asymptotic solution

Y. S. M. Morsi* and B. R. Clayton†

An asymptotic solution of the momentum equation is given that describes the decay of swirling flow passing along the annulus formed between two concentric, straight, circular-section pipes having a common starting point. The flow is considered turbulent and approximations are made consistent with the notion of fully developed flow conditions. Applications of this approach are reviewed and shortcomings highlighted. A series of calculations are presented and compared with experimental and theoretical data previously obtained by the authors. It is shown that acceptable predictions of the overall flow behavior can be obtained over a wide range of initial conditions provided the calculations procedure is applied in regions of validity, which has not been the case in some published work. Substantial errors are found if, for example, the procedure is allowed to commence at inlet to the annulus owing to the inconsistency of the assumptions in the initially developing-flow region, which for this work extends at least five outer-pipe diameters downstream from inlet. The authors' previous numerical integration scheme may be used to predict flows satisfactorily in the developing-flow region and the present asymptotic solution used subsequently to reduce computation time and cost.

Keywords: *turbulence, swirl, annuli, concentric tubes, swirl decay, asymptotic solution*

Introduction

The behavior of turbulent swirling flow along the annulus formed between two concentric cylinders we have already described[1,2] using experimental data. A numerical analysis using various turbulence models has been developed[3] to predict the variation of the principal flow parameters from specified or measured inlet conditions. The accuracy of the technique was discussed along with its validity of application.

In this paper, we present an asymptotic solution of the momentum equation that is mainly concerned with the development and subsequent decay of turbulent swirling flow in an annulus. We will demonstrate that such a solution can give a fast and adequate prediction of the main characteristics of turbulent swirling flow although complete generality is not possible; indeed, excessive computation would be required to achieve this. Approximations are kept to a minimum and are fully justified.

Several studies on swirling flow have been reported previously, but these were mainly concerned with the decay of swirl in pipes. The early analyses were restricted to laminar flow owing to the limited capacity of computers at that time. A description of turbulent swirling flow at each point in an annulus, including all turbulent components and stresses at both walls, requires the solution of five partial differential equations, as was shown in a previous numerical analysis.[3] This solution is mathematically complex, requiring large CPU times and computers. Although some workers have simplified the general governing equations to reduce the complexity of solutions, doing so can lead to errors in predictions. In the following review, we illustrate the deficiencies of previous work and thus allow a definition of the terms of reference leading to our analysis.

* Now at Water Research Laboratory, University of New South Wales, Manly Vale, NSW 2093, Australia
† Department of Mechanical Engineering, University College London, Torrington Place, London WC1E 7JE, UK
Received 23 May 1986 accepted for publication 25 March 1987

0142-727X/87/040293-10$03.00

Review and appraisal

Talbot[4] was probably the first to publish an analysis of steady, laminar, swirling flow of a constant property fluid in a straight pipe of circular cross-section. This work commenced before the advance of large-capacity, high-speed computers, so attention was focused on small perturbations from Poiseuille flow. Based on the coordinate system and component velocities of Figure 1, and assuming rotational symmetry, the Navier-Stokes equations may be written in the form

$$\bar{V}\frac{\partial \bar{V}}{\partial r}+\bar{U}\frac{\partial \bar{U}}{\partial x}-\frac{\bar{W}^2}{r}=-\frac{1}{\rho}\frac{\partial p}{\partial r}+\nu\left(\nabla^2\bar{V}-\frac{\bar{V}}{r^2}\right) \tag{1}$$

$$\bar{V}\frac{\partial \bar{W}}{\partial r}+\bar{U}\frac{\partial \bar{W}}{\partial x}+\frac{\bar{V}\bar{W}}{r}=\nu\left(\nabla^2\bar{W}-\frac{\bar{W}}{r^2}\right) \tag{2}$$

$$\bar{V}\frac{\partial \bar{U}}{\partial r}+\bar{U}\frac{\partial \bar{U}}{\partial x}=-\frac{1}{\rho}\frac{\partial p}{\partial x}+\nu\nabla^2\bar{U} \tag{3}$$

and the corresponding continuity equation is

$$\frac{\partial \bar{V}}{\partial r}+\frac{\bar{V}}{r}+\frac{\partial \bar{U}}{\partial x}=0 \tag{4}$$

Equation (2) may be simplified by considering the axial velocity $\bar{U}$ to differ from that in Poiseuille flow U_p, by a small perturbation $\Delta\bar{U}$, that is,

$$\bar{U}=U_p+\Delta\bar{U} \tag{5}$$

where

$$U_p=\hat{U}\left[1-\left(\frac{r}{r_0}\right)^2\right] \tag{6}$$

and $\hat{U}$ represents the maximum velocity on the pipe centerline. Assuming all the terms involving $\Delta\bar{U}$ and the radial velocity $\bar{V}$ are neglected on the basis of an order of magnitude argument,

Eq. (2) may be linearized to form the *swirl* equation

$$\bar{U}_p \frac{\partial \bar{W}}{\partial x} = \nu\left(\nabla^2 \bar{W} - \frac{\bar{W}}{r^2}\right)$$

$$= \nu\left(\frac{\partial^2 \bar{W}}{\partial r^2} + \frac{1}{r}\frac{\partial \bar{W}}{\partial r} + \frac{\partial^2 \bar{W}}{\partial x^2} - \frac{\bar{W}}{r^2}\right) \quad (7)$$

Equation (7) suggests a solution for $\bar{W}$ can be found by separating variables. When this is done, the equation of motion can be reduced to a standard form of the confluent hypergeometric equation. The solution of this equation automatically satisfies the inner boundary condition, namely, that $W=0$ on the pipe axis. The second condition, $W=0$ at the pipe walls, is used to determine the eigenvalues as functions of Reynolds number. A momentum integral analysis was also used by Talbot[4] to estimate the radial velocity and the perturbations on the Poiseuille-flow axial velocity, but his results are limited to a very large distance from the entry region.

The analytical approach developed by Wolf *et al.*[5] was initiated by earlier observations of a reversal of the axial velocity at the centerline of a pipe containing swirling through-flow. However, a strong swirl is needed to develop such a flow reversal, so Talbot's analysis was inappropriate. Thus consideration was given[5] to flows both along a pipe rotating about its axis of symmetry and to swirling flows along stationary pipes. The analysis was based on a perturbation about a flow undergoing solid-body rotation (forced-vortex) with an axial Reynolds number of zero. With a small through-flow (small-axial Reynolds number), an analytical solution of the tangential components of the linearized Navier-Stokes and vorticity transport equations was obtained by taking as finite the product of the Reynolds number and the square of the swirl ratio (the ratio of the tangential velocity of the rotating tube to the mean axial velocity). The use of Fourier integrals led to a transformation of the equations of motion, and the inverse Fourier transforms of the solution of the transport equations allowed expressions for the vorticity and velocity components to be obtained in terms of zero and first-order Bessel functions. A numerical technique, based on an iterative scheme using central finite differences for all derivatives with respect to radial distance, was also developed. The axial distance along the pipes, from the junction between the moving pipe and the stationary pipe, was transformed by a mapping function to maintain numerical accuracy with a fixed number of grid points. The kinematic equations were then solved with the required boundary conditions, and the variations of pressure subsequently deduced by integrating the axial and radial components of the Navier-Stokes equations. The results of Wolf *et al.*[5] coincide with those of Talbot[4] at distances well downstream from the pipe entrance.

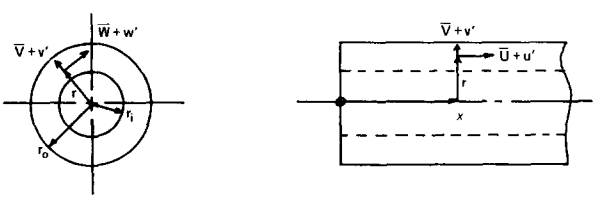

Figure 1 Coordinate system

Kiya *et al.*[6] examined steady laminar swirling flow in the entrance region of a pipe, where the flow development was most rapid. The investigation commenced from Eqs. (1–3) and then, by assuming a boundary-layer type flow, the equation of motion was simplified on the basis of an order of magnitude analysis. The energy equation was also included so that the effect of swirl on the temperature of the fluid could be found for a constant wall temperature. (Throughout this work, we considered air of constant Prandtl number 0.72 and only isothermal flows, so no further discussion of the energy equation is necessary here.) Combining the wall and axis boundary conditions allowed integration of both the continuity equation and the approximated form of Eq. (1), namely,

$$\frac{\partial p}{\partial r} = \rho \frac{\bar{W}^2}{r} \quad (8)$$

Expressions for $\partial p/\partial r$ and the radial and tangential velocities were then substituted into the approximated form of Eqs. (2) and (3). Since the resulting equations were of partial integro-

Notation

$A, A_n, a, a_n, B, b_n, C, C_n, c_n, D_n, n$	Various constants
F	Operator, $\frac{d^2}{dR^2}+\frac{1}{R}\frac{d}{dR}-\frac{1}{R^2}$
$J_1(\lambda_n^* R)$	Bessel function of first order and first kind
L	$X/\{\mathrm{Re}/(1+\varepsilon')\}$
$M(R), M^*(R)$	Eigenfunctions
M_1	Eq. (36)
$\bar{M}$	Dimensionless angular momentum, WR
m	$\lambda_n^2/\lambda_n^{*2}$
$N(L)$	$B\exp(-\lambda_n^2 L)$
P	$p/\frac{1}{2}\rho U_{av}^2$
p	Gauge pressure
Q	Volume flow rate
R	r/r_0
Re	Reynolds number, $U_{av} r_0/\nu$
$\hat{R}$	Value of R at which W is a maximum
r	Radius
r_i	Inner radius
r_0	Outer radius
S	Swirl intensity, Eq. (40)
S_1, S_7	Values of S at stations 1 and 7, respectively
U	$\bar{U}/U_{av}$
U_{av}	Average axial velocity, $Q/\pi(r_0^2-r_i^2)$
$\bar{U}$	Time mean axial velocity
$\hat{U}$	Maximum velocity in Poiseuille flow
$\Delta\bar{U}$	$\bar{U}-U_p$
U_p	Local velocity in Poiseuille flow
u'	Fluctuating axial velocity
$\bar{V}$	Time mean radial velocity
v'	Fluctuating radial velocity
W	$\bar{W}/U_{av}$
$\bar{W}$	Time mean tangential velocity
w'	Fluctuating tangential velocity
$\rho\overline{u'w'}, \rho\overline{v'w'}$	Reynolds stresses
X	x/r_0
x	Axial distance from inlet
$Y_1(\lambda_n^* R)$	Bessel function of first order and second kind
α	Radius ratio, r_i/r_0
ε	Eddy kinematic viscosity of fluid, μ_t/ρ
ε'	ε/ν
λ_n, λ_n^*	Eigenvalues
μ	Dynamic viscosity of fluid
μ_t	Turbulence (eddy) viscosity of fluid
ν	Kinematic viscosity of fluid, μ/ρ
ν_e	Effective kinematic viscosity of fluid, $\nu+\varepsilon$
ρ	Density of fluid
Ψ	Guide vane setting angle

differential form, they are unlikely to possess a general analytical solution.

To avoid perturbation techniques or linearization of the inertia terms, a finite difference method was developed by Kiya *et al.*[6] so that errors within the entrance region were minimized. The subsequent iteration procedure was applied to the axial and tangential velocity components and the pressure along the pipe axis. Results were obtained for initial swirl distributions of the forced-vortex type superimposed on uniform axial flow, and it was shown that the presence of swirl substantially increased the entrance length and reduced the centerline pressure drop along the pipe axis in the fully developed region. The swirl intensity, defined as the ratio of angular momentum to axial momentum, was found to decay exponentially in the fully developed region (where the centerline axial velocity is, say, within 1% of the value at infinity), but the decay was considerably more rapid in the entrance region.

Scott[7] simplified Eq. (2) to produce a swirl equation given by

$$U_{av}\frac{\partial \bar{W}}{\partial x}=v_e\left(\frac{\partial^2 \bar{W}}{\partial r^2}+\frac{1}{r}\frac{\partial \bar{W}}{\partial r}-\frac{\bar{W}}{r^2}\right) \tag{9}$$

and applied this to flow along the annulus formed between two concentric pipes having a ratio of inner to outer radii of 0.4. Equation (9) was considered to describe flow in the region where variations of velocity along the annulus were small relative to the variations in the radial direction. Furthermore, since the tangential velocity ultimately decayed to zero for very large x, the average axial velocity U_{av} was constant. What is not known, however, is where these conditions apply in the annulus. Thus the differences between Eq. (9) and the equivalent equation used by Talbot,[4] our Eq. (7), are (a) on the left-hand side, U_{av} is constant, where $\bar{U}$ is a function of r, and (b) on the right-hand side, $\partial^2 \bar{W}/\partial x^2$ is omitted from Eq. (9). Scott cast Eq. (9) into a dimensionless form and then used the method of separating variables for the dimensionless tangential velocity $W=\bar{W}/U_{av}$. The general solution of the equation comprised the product of an infinite series containing Bessel functions of the first order and of the first and second kinds (because the known boundary conditions $\bar{W}=0$ apply at both the inner and outer walls) and an integral that was evaluated across the annulus. This integral contained the product $r\bar{W}(0,r)$, where $\bar{W}(0,r)$ represents the swirl velocity at the inlet. A simple solution thus occurred for free-vortex flow because the product is then a constant.

Unfortunately, the previous assumptions regarding orders of magnitude are invalid in the entrance region, and so the subsequent accuracy of the solution must be open to question. The solution should commence at a value of x that corresponds to the start of the fully developed region, but this is generally unknown; furthermore, free-vortex flow does not then exist. The main limitation of Scott's technique lies in the absence of data on the location of the starting point for its accurate use. Nevertheless, if a numerical technique for the solution of more accurate equations of motion were used to ascertain the flow behavior in, and the extent of, the developing region, the asymptotic solution could be used subsequently with a considerable saving in computation effort and time but with no loss of accuracy. This is the basis of our investigation, in which a constant viscosity model is subsequently adopted. A general analysis of turbulent swirling flows lie in the choice of a suitable swirling flow in a constant area axisymmetric annulus has already been presented,[3] and we will make use of these results when comparing accuracies of prediction. We have previously pointed out that the principal difficulties associated with the analysis of turbulent swirling flows lies in the choice of a suitable eddy viscosity model and the increased complexity of the equation of motion. Great care is needed if orders of magnitude analyses are not to lead to erroneous simplifications, inconsistencies, and possible numerical instabilities in the solution of the resulting equations.

Kreith and Sonju[8] examined turbulent swirling flow in a pipe by simplifying the Navier-Stokes equations using an order of magnitude analysis based on experimental evidence. Some of the experiments considered were not strongly related to the theoretical development but were accepted in the absence of more relevant data. In particular, the eddy kinematic viscosity ε was assumed to be spatially independent throughout the flow field. Moreover, perturbations on the axial velocity were assumed negligible so that $\bar{U}$ was taken to be a function of r only; that is, the fully developed axial velocity profile was used. The resulting swirl equation is then given by

$$\bar{U}\frac{\partial \bar{W}}{\partial x}=(v+\varepsilon)\left(\frac{\partial^2 \bar{W}}{\partial r^2}+\frac{1}{r}\frac{\partial \bar{W}}{\partial r}-\frac{\bar{W}}{r^2}\right) \tag{10}$$

We see that since ε is constant, the special case of constant $\bar{U}$, represented by the average velocity U_{av}, reduces Eq. (10) to Eq. (9), which is the same as that investigated by Scott.[7] In their calculations, Kreith and Sonju actually used the expression $\bar{U}=\hat{U}(1-r/r_0)^{1/7}$. This approach gave greater accuracy in the subsequent solution of Eq. (10) following separation of variables and adoption of a method of approximations.

The theory developed by Kreith and Sonju[8] was applied to swirling flow induced by a helical tape inserted the length of a tube; thus the initial swirl distribution and the expression for ε were deduced for that case using related experimental data. The correlation equation for ε was written in the form $\varepsilon=A(\mathrm{Re})^n$, where A and n are constants, and Re represents the axial-flow Reynolds number. It was recognized that this empirical relationship, in which ε is taken to be a function only of Re, was not really satisfactory, but subsequent correlations show good agreement occurred between the average measures of swirl decay and theoretical predictions.

Similarity criteria were used by Rochino and Lavan[9] in the derivation of a simplified equation of motion for turbulent swirling flow along circular-section pipes. They thus automatically restricted their results to fully developed flow, and so employed the same $\bar{U}$ variation as Kreith and Sonju.[8] The similarity criteria adopted were essentially extensions of Von-Karman's hypothesis and gave rise to several conditions relating the length scale to the mean tangential velocity and its derivatives. Equation (10) was used[9] to determine $\bar{W}$, except that an additional term $\partial^2 \bar{W}/\partial x^2$ was retained in the second set of parentheses on the right-hand side of the equation. This appears at odds with the assertions concerning orders of magnitude, although it seems the term was subsequently discarded. Values of the constants, which inevitably arise in similarity relationships, were derived from previous work on swirling flow in pipes. It was, however, necessary to include a discontinuity in the empirical relations describing the eddy kinematic viscosity to ensure it vanished at the wall. Despite the extensive empiricism and averaging of input data, comparisons between the theoretical predictions and measurements (obtained by other workers) appear to be good overall at distances well downstream from the pipe entry. Even so, it is most unlikely that this approach[9] can be generalized or that accurate details of the flow near the entry and the walls can be obtained.

From the foregoing, it is evident that attempts to simplify the approach to, and subsequent calculations to describe, the behavior of swirling flows in pipes and annuli cannot be generalized and may lead to significant inaccuracies. An attempt to overcome these problems has been described by Morsi and Clayton.[3] The purpose of the following treatment is to show a simplified analysis can be used accurately only in conjunction with complex analysis covering the initial stages of flow development of a freely decaying swirl flow downstream from the entry to an annulus between two concentric pipes of circular cross-section.

An asymptotic solution

Although a complete solution of the Navier-Stokes equations for turbulent flow is as yet unobtainable, an approximate

solution for the decay of swirl in an annulus can be deduced from the tangential momentum equation without fully solving all the equations. The derivation of the relevant equation is as follows, and the method may be considered an algebraic solution.

For incompressible turbulent flow, the Navier-Stokes equations can be written in cylindrical coordinates (Figure 1), of which the tangential component of rotationally symmetric flow with negligible body forces becomes

$$\bar{U}\frac{\partial \bar{W}}{\partial x}+\bar{V}\frac{\partial \bar{W}}{\partial r}+\frac{\bar{W}\bar{V}}{r}$$
$$=\nu\left[\nabla^2\bar{W}-\frac{\bar{W}}{r^2}\right]-\left[\frac{\partial}{\partial x}(\overline{u'w'})+\frac{\partial}{\partial r}(\overline{v'w'})+2\frac{(\overline{v'w'})}{r}\right] \quad (11)$$

Equation (11) may be referred to as the *swirl* equation and will be simplified and solved after adopting the following assumptions:

1. The flow is fully developed; that is, the decay of the axial velocity component is negligible in comparison with the decay of the swirl velocity component.
2. The radial velocity component is very much smaller than both the axial and the tangential velocity components.
3. Since $\partial^2\bar{W}/\partial x^2$ tends to zero asymptotically for large Reynolds numbers according to Talbot[4] and Kreith and Sonju,[8] and owing to the constant momentum distribution in the radial direction, one may take $(\bar{V}\partial\bar{W}/\partial r+\bar{W}\bar{V}/r)\rightarrow 0$.
4. The decay of $\partial(\overline{u'w'})/\partial x$ is much smaller than that of $\bar{U}(\partial\bar{W}/\partial x)$.
5. *Reynolds stress* $\rho\overline{v'w'}$ can be approximated by $-\mu_t(\partial\bar{W}/\partial r-\bar{W}/r)$.
6. The eddy kinematic viscosity $\varepsilon=\mu_t/\rho$ does not change appreciably with r or x and may be considered constant throughout the flow.
7. The basic structure of the $\rho\overline{v'w'}$ term does not change from one vortex system to another according to Kreith and Sonju.[8]

Using the preceding assumptions and inserting the approximate value of Reynolds stress in the swirl equation, there results

$$\bar{U}\frac{\partial \bar{W}}{\partial x}=(\nu+\varepsilon)\left(\frac{\partial^2\bar{W}}{\partial r^2}+\frac{1}{r}\frac{\partial\bar{W}}{\partial r}-\frac{\bar{W}}{r^2}\right) \quad (12)$$

It will be convenient to form dimensionless parameters by introducing the following ratios:

$$U=\frac{\bar{U}}{U_{av}} \qquad W=\frac{\bar{W}}{U_{av}} \qquad \mathrm{Re}=\frac{U_{av}}{\nu}$$
$$\varepsilon'=\frac{\varepsilon}{\nu} \qquad X=\frac{x}{r_0} \qquad L=\frac{X}{\{\mathrm{Re}/(1+\varepsilon')\}} \quad (13)$$
$$R=\frac{r}{r_0} \qquad \alpha=\frac{r_i}{r_0} \qquad P=\frac{p}{\frac{1}{2}\rho U_{av}^2}$$

where Re represents the Reynolds number of the flow, and α the radius ratio. Equation (12) then takes the form

$$U\frac{\partial W}{\partial L}=\frac{\partial^2 W}{\partial R^2}+\frac{1}{R}\frac{\partial W}{\partial R}-\frac{W}{R^2} \quad (14)$$

Equation (14) can be solved by applying the method of separation of variables so that we may write

$$W=M(R)N(L) \quad (15)$$

Thus Eq. (14) reads

$$\frac{1}{N}\frac{dN}{dL}=\frac{1}{UM}\left\{\frac{d^2M}{dR^2}+\frac{1}{R}\frac{dM}{dR}-\frac{M}{R^2}\right\} \quad (16)$$

The left-hand side of Eq. (16) is a function only of L, and the right-hand side a function only of R. The equality in this equation can be valid only if both sides of the equation are equal to the same constant, $-\lambda_n^2$, for example. Equation (16) then becomes

$$\frac{1}{N}\frac{dN}{dL}=-\lambda_n^2=\frac{1}{UM}\left\{\frac{d^2M}{dR^2}+\frac{1}{R}\frac{dM}{dR}-\frac{M}{R^2}\right\} \quad (17)$$

where $-\lambda_n^2$ are the eigenvalues and $M(R)$ the eigenfunctions.

It is apparent from Eq. (17) that three different possibilities arise for the values of $-\lambda_n^2$, namely, $-\lambda_n^2>0$, $-\lambda_n^2=0$, and $-\lambda_n^2<0$. However, it was shown by Kreith and Sonju[8] that the only valid solution is $-\lambda_n^2<0$, and so Eq. (17) reduces to

$$\frac{d^2M}{dR^2}+\frac{1}{R}\frac{dM}{dR}+\left(\lambda_n^2U-\frac{1}{R^2}\right)M=0 \quad (18a)$$

and

$$\frac{dN}{dL}=-N\lambda_n^2 \quad (18b)$$

These two equations can now be solved individually. Equation (18b) has a solution of the form

$$N=B\exp(-\lambda_n^2L) \quad (19)$$

where B is a constant. This shows the swirl velocity component decays exponentially along the length of the annulus as deduced from the physical behavior of the flow.[2]

Experimental work[1,10] has indicated the velocity distribution displays an almost uniform pattern except near the walls. Since U is a dimensionless quantity, the combination $U-1$ can be taken as a perturbation factor noting that $|U-1|$ is unity at the concave and convex walls but decreases to zero close to the outer edge of the boundary layer on each wall. This permits us to introduce a perturbed equation as follows:

$$F(M)+|U-1|\lambda_n^2M+\lambda_n^2M=0 \quad (20)$$

compared with an unperturbed equation

$$F(M^*)+\lambda_n^{*2}M^*=0 \quad (21)$$

where we have introduced the operator $F\equiv d^2/dR^2+(1/R)(d/dR)-1/R^2$. The eigenvalues λ_n, λ_n^* and the eigenfunctions M, M^* of Eqs. (20) and (21), respectively, may be expanded as follows:

$$\lambda_n^2=\lambda_n^{*2}+(U-1)P_n+(U-1)^2Q_n+(U-1)^3R_n+\cdots+ \quad (22)$$

and

$$M=M^*+(U-1)p_n+(U-1)^2q_n+(U-1)^3r_n+\cdots+ \quad (23)$$

where P_n, Q_n, R_n are eigenvalues, and p_n, q_n, r_n are eigenfunctions.

The values of λ_n^2 and M for the core region, that is, away from the concave and convex walls, have been deduced by Morsi[11] in the form

$$\lambda_n^2=\frac{\lambda_n^{*2}}{U} \quad (24)$$

and

$$M=M^* \quad (25)$$

However, for the points close to the walls, it has been shown[11]

$$\lambda_n^2=m\lambda_n^{*2} \quad (26)$$

and

$$M=M^* \quad (27)$$

where m is the number of terms in the series (Eq. 22). From the previous relation, it is apparent that it is sufficient to determine the λ_n^* and M^* of the unperturbed differential equation (Eq. 21) to obtain the λ_n and M of the perturbed differential equation (Eq. 20). Furthermore, the general solution of the unperturbed equation (Eq. 21) is available[12] and takes the form

$$M^*=a_nJ_1(\lambda_n^*R)+b_nY_1(\lambda_n^*R) \quad (28)$$

where a_n and b_n are arbitrary constants, J_1 is the first-order

Bessel function of the first kind, and Y_1 is the first-order Bessel function of the second kind.

Solutions for the two variables may now be gathered together so that the tangential velocity may be expressed in the form

$$W(R, L)=\sum_{n=1}^{\infty} \exp(-\lambda_n^2 L)\left[C_n J_1(\lambda_n^* R)+D_n Y_1(\lambda_n^* R)\right] \quad (29)$$

where $C_n = Ba_n$ and $D_n = Bb_n$ are arbitrary constants.

Boundary conditions

At the inlet

The velocity at the entrance, $W(R, 0)$ may be expressed in the form

$$W(R, 0)=c_0 R^{-1}+c_1+c_2 R+c_3 R^2+\cdots+c_n R^{n-1} \quad (30)$$

Equation (30) includes three different and particularly important types of flow, namely, free vortex, forced vortex, and a linear combination of both.

At the walls

The swirl velocity at the inner and outer walls must be zero, that is,

$$W(\alpha, L)=0 \quad (31a)$$

and

$$W(1, L)=0 \quad (31b)$$

since $R=\alpha$ at the inner wall and is unity at the outer wall. Using these conditions and the value of λ_n^2 on the walls from Eq. (26), in Eq. (29), we obtain

$$W(\alpha, L)=\sum_{n=1}^{\infty} \exp(-m\lambda_n^{*2} L)[C_n J_1(\lambda_n^*\alpha)+D_n Y_1(\lambda_n^*\alpha)] \quad (32)$$

Since $\exp(-m\lambda_n^{*2} L)$ cannot be zero for an arbitrary L, and because M^* is an orthogonal function[12] it can be shown

$$C_n J_1(\lambda_n^*\alpha)+D_n Y_1(\lambda_n^*\alpha)=0$$

or

$$D_n=-\frac{C_n J_1(\lambda_n^*\alpha)}{Y_1(\lambda_n^*\alpha)} \quad (33)$$

Inserting the value of D_n into Eq. (29) gives

$$W(R, L)=\sum_{n=1}^{\infty} A_n \exp(-\lambda_n^2 L)[Y_1(\lambda_n^*\alpha)J_1(\lambda_n^* R) - J_1(\lambda_n^*\alpha)Y_1(\lambda_n^* R)] \quad (34)$$

where

$$A_n=\frac{C_n}{Y_1(\lambda_n^*\alpha)}$$

From the boundary condition at the inlet, one has

$$W(R, 0)=\sum_{n=1}^{\infty} A_n M_1 \quad (35)$$

where

$$M_1 = Y_1(\lambda_n^*\alpha)J_1(\lambda_n^* R)-J_1(\lambda_n^*\alpha)Y_1(\lambda_n^* R) \quad (36)$$

Since M_1 is an orthogonal function with respect to the weighting function R, the Sturm Liouville theorem[12] may be used to write

$$A_n=\frac{\int_\alpha^1 R M_1 W(R, 0)dR}{\int_\alpha^1 R M_1^2 dR} \quad (37)$$

Details of the evaluation of the function A_n have been described by Morsi.[11]

Finally, the general equation for the dimensionless swirl velocity at an arbitrary point, other than on the walls, may be obtained by substituting λ_n^2 from Eq. (24) and A_n from Eq. (37) into Eq. (34) to give

$$W(R, L)=\sum_{n=1}^{\infty} A_n \exp\left(\frac{-\lambda_n^{*2} L}{U}\right)[Y_1(\lambda_n^*\alpha)J_1(\lambda_n R) - J_1(\lambda_n^*\alpha)Y_1(\lambda_n^* R)] \quad (38)$$

General discussion of calculation procedures

In this section, we discuss the computer programs associated with the general solution of the swirl equation (Eq. 38) used to predict the decay of the tangential velocity components along the annulus. We also present some of the results obtained.

The eigenvalues λ_n^* are determined from the zeros of

$$W(1, L)=Y_1(\lambda_n^*\alpha)J_1(\lambda_n^*)-J_1(\lambda_n^*\alpha)Y_1(\lambda_n^*) \quad (39)$$

NAG routines (available within the UCL computer library) were used to evaluate approximations of the Bessel functions of the first and second kind, for example, $J_0(\lambda_n^*)$, $Y_0(\lambda_n^*)$, $J_1(\lambda_n^*)$, $Y_1(\lambda_n^*)$; $J_0(\lambda_n^*\alpha)$, $Y_0(\lambda_n^*\alpha)$, $J_1(\lambda_n^*\alpha)$, $Y_1(\lambda_n^*\alpha)$; and so on.

A computer program was written to perform the iteration of a cycle to satisfy Eq. (39) for different values of λ_n^* and $\lambda_n^*\alpha$ for $\alpha=0.51$ and 0.61. Table 1 shows the results of these calculations. Another computer program was developed to solve Eq. (38) analytically for different values of α, Re, and Ψ, the swirl blade angle.[1] (The program can also be modified to provide a solution for swirling flow in pipes.) The program starts functioning by fitting the inlet tangential velocity profile to a polynomial function with the aid of the NAG library routine and then computes the radial distribution of the tangential velocity profiles along the annulus. The swirl intensity S, defined as the ratio of total angular momentum to the total axial momentum of the fluid at a given station along the annulus, can be calculated from

$$S=\frac{\int_{r_i}^{r_0} \bar{U}\bar{W}r^2 dr}{\int_{r_i}^{r_0} \bar{U}^2 r dr} \quad (40)$$

The velocity and swirl intensity profiles are then subsequently plotted.

In this analytical solution the eddy kinematic viscosity ε is assumed to be spatially independent and a function only of Reynolds number that takes the form

$$\frac{\varepsilon}{\nu}=\varepsilon'=C(\mathrm{Re})^a$$

where C and a are constants that depends on the type of flow and configurations under consideration. For a pipe flow, Kreith and Sonju[8] found the constant C had the value of 4.15×10^{-3}, whereas the constant a had the value of 0.86 in the Reynolds number range $1.8-6.1\times10^4$.

Table 1 Calculated eigenvalues λ_n^* for different radius ratios α

n	0.30	0.40	0.50	0.51	0.61
1	4.7052	5.3911	6.3931	6.5184	8.1283
2	9.1042	10.5577	12.6247	12.8786	16.1470
3	13.5532	15.7664	18.8889	19.2721	24.1907
4	18.0199	20.9882	25.1624	25.6740	32.2280
5	22.4948	26.2155	31.4397	32.0800	40.2280
6	26.9736	31.4456	37.7189	38.4877	48.2280
7	—	—	—	44.8961	56.3960
8	—	—	—	51.3055	64.4505
9	—	—	—	57.7153	72.5040
10	—	—	—	64.1254	80.5580
11	—	—	—	70.5358	88.6130
12	—	—	—	76.9463	96.6667

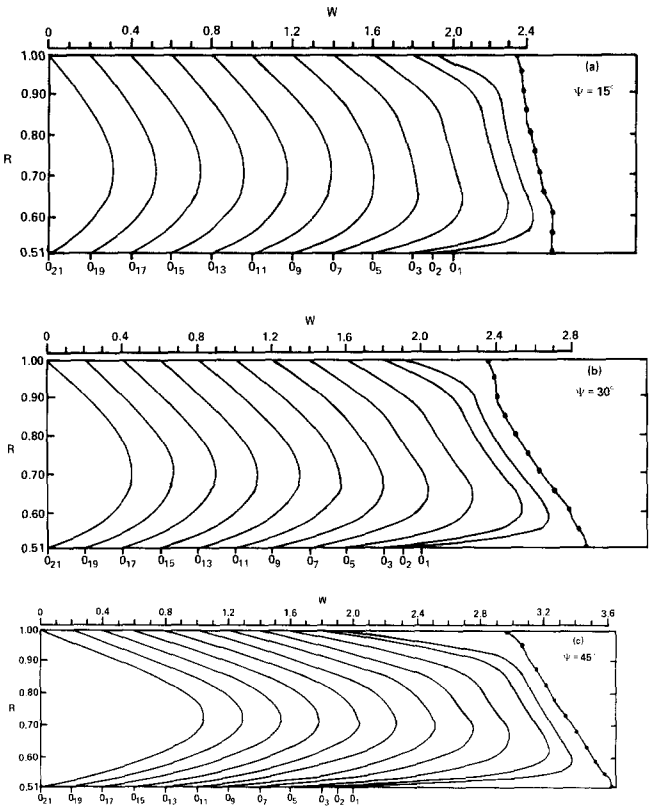

Figure 2 Computed dimensionless tangential velocity profiles in annulus commencing from station 1 for $\alpha=0.51$ and Re = 28 700. (These values of α and Re apply to all subsequent figures unless stated otherwise.)

In this study, a technique similar to that used by Wolf *et al.*[5] and Scott[7] has been adopted to deduce ε'. The tangential velocity profiles at a given station are parameterized with respect to the dimensionless variable L, which as shown in Eq. (13), contains x, Re, and ε', and so one can deduce the best fit for ε' from comparing the analytical and experimental profiles. By carrying out this procedure for two different Reynolds numbers, namely, 28 700 and 22 400, the following relation for ε' was found to hold good:

$$\varepsilon' = 0.404(\mathrm{Re})^{0.305} \tag{41}$$

It is interesting to note that in the analysis of an actuator disc model of an axial compressor, Hawthorne and his coworkers[13,14] developed an equation similar to Eq. (38) to describe the exponential decay of radial velocity of an inviscid fluid passing through an annulus. The presence of a radial velocity results from a radial shift of streamlines, but circumferential (swirl) velocities were regarded as negligible in the linear theory. Applying appropriate boundary conditions leads to an equation identical to Eq. (39) for the determination of the eigenvalues. It is pointed out that an approximate solution for the zeros of Eq. (39) is given by

$$\lambda_n^* \approx \frac{n\pi}{1-\alpha} \tag{42}$$

in our notation, where n is a positive integer. Table 1 shows this approximate solution improves for all α as n becomes large but still represents good accuracy for the first term corresponding to $n=1$. This point was not apparently appreciated by Scott,[7] who stated that for n large, the difference in successive eigenvalues exhibited by his numerical analysis of the case $\alpha=0.4$ approximated 5.236, which is, of course, identical to $\pi/0.6$.

Equations (38) and (41) then show, with the approximation (Eq. 42), the first term in the series for $W(R, L)$ decays as

$$\exp\left\{-\left(\frac{\pi}{1-\alpha}\right)^2 \frac{X}{\mathrm{Re}} \frac{(1+\varepsilon')}{U}\right\} = \exp\left\{\frac{-0.01468X}{U}\right\} \tag{43}$$

Since the asymptotic theory does not apply accurately until the flow is fully developed, that is, until U is a function only of R, Eq. (43) should strictly be used to ascertain the exponential decay of swirl beyond the value of X corresponding to fully developed flow. The exponential decay function would then read

$$\exp\left\{\frac{-0.01468(X-9.9)}{U}\right\}$$

since $X=9.9$ for fully developed flow as stated later. Detailed confirmation of this type of decay with the first-term dominant requires substantial analysis and has not yet been checked rigorously, but further examination of the data described in the next section certainly lends support to this contention. Nevertheless, it would be quite misleading to overemphasize the analogy between the actuator disc problem and the present problem, since the first is concerned with inviscid flow and radial velocities, and the latter is clearly not.

Results

Figures 2 and 3 show the computed tangential velocity profiles in dimensionless form for different Re, Ψ, and α. Station 1 corresponds to $X=0$, and the remaining stations are at consecutive intervals of 1.65. Two initial conditions were examined to estimate the effect of initial conditions on the radial distributions of tangential velocity and the subsequent decay of swirl along the annulus. For the first condition, the experimental, nearly free-vortex initial swirl distribution at station 1 was used, and the results in Figure 2 show the initial

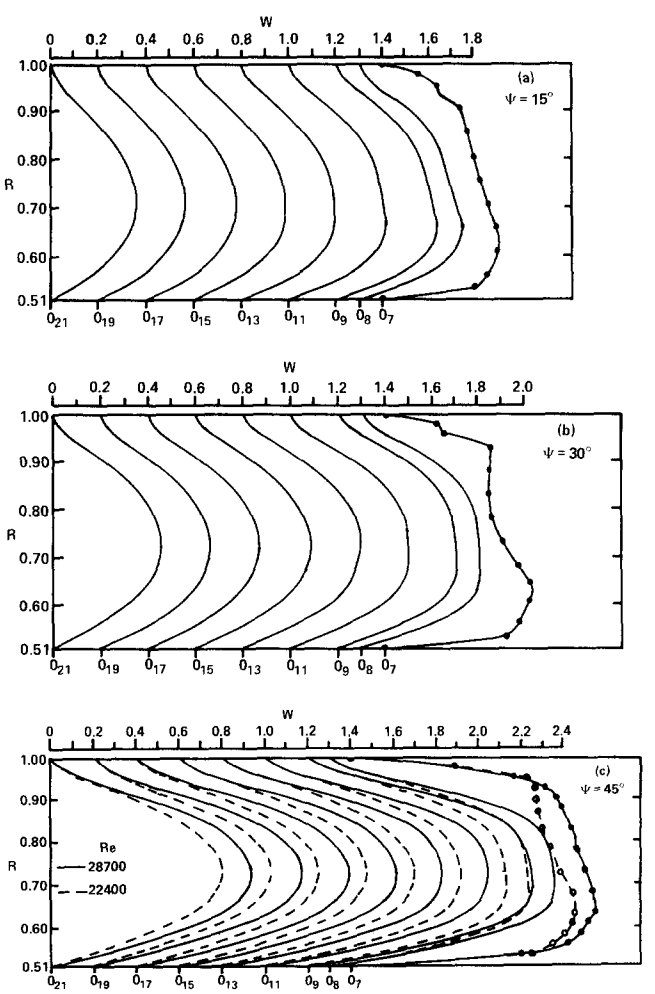

Figure 3 Computed dimensionless tangential velocity profiles in annulus commencing from station 7

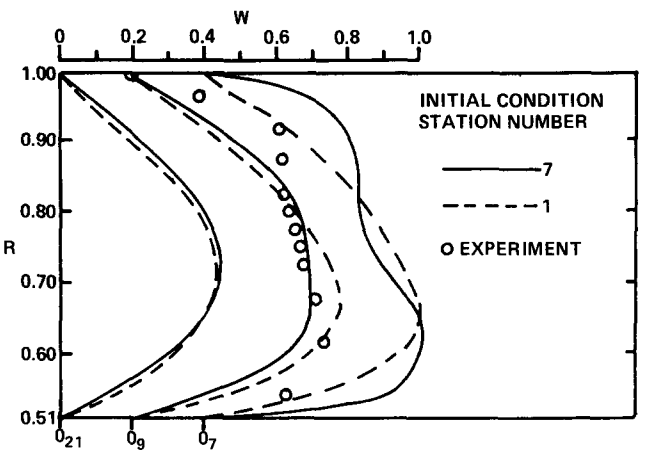

Figure 4 Comparison of predicted dimensionless tangential velocity profiles for $\Psi = 30°$

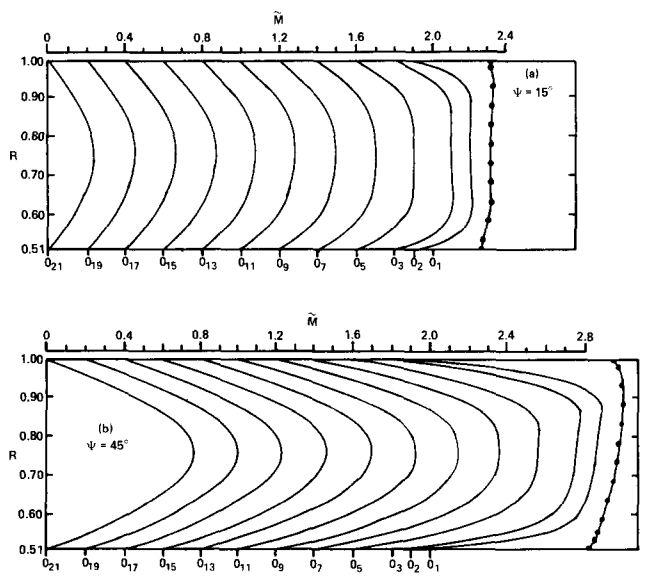

Figure 5 Computed distribution of dimensionless angular momentum in annulus commencing from station 1

free-vortex character is rapidly lost. The location of maximum swirl velocity moves radially toward the concave wall and is, for example, located at a value of $\hat{R} = 0.71$ at station 19 ($X = 29.70$) for $\Psi = 15°$ and Re = 28 700. Unless stated otherwise, all the results shown in the following figures refer to $\alpha = 0.51$ and Re = 28 700.

For the second initial condition, the experimental tangential velocity profile at station 7 was used corresponding to the fully developed region. The results shown in Figure 3 illustrate a behavior similar to that of the first case. However, compared with the first case, the location of $\hat{R}$ is slightly closer to the concave wall and has a value of 0.715 for $\Psi = 15°$. The effects of changes in Re and Ψ are also shown in Figure 3. It can be seen that $\hat{R}$ increases, that is, moves toward the outer concave wall, as Re decreases and Ψ increases.

An investigation was carried out to examine the influence of the two initial conditions on the tangential velocity distribution further downstream in the fully developed flow region of the annulus. It can be seen from the results of Figure 4, which represent a typical swirl angle of 30°, that the discrepancies between the two predicted profiles are significant, particularly at the beginning of the fully developed region of the flow at station 7. The effect of the initial conditions on the pattern of the profiles downstream diminishes as the swirl progressively decays. However, even at station 21, there is evidently still a significant difference between the two profiles in both shape and magnitude. Figure 4 also shows a comparison between the two predicted tangential velocity profiles at station 9 and corresponding measured data.[1] The predicted profile starting from initial conditions at station 7 is evidently in closer agreement with experimental data than that predicted from the profile at station 1. The profile from the latter prediction is more peaky, and there are significant differences between the measured and predicted values particularly near the outer wall. This behavior may be attributed to the stronger influence of the shear and normal stresses on the development of the flow in the inlet and rapidly decaying regions than that in the fully developed region where the flow starts to decay exponentially.

The capability of the algebraic solution to predict the physical behavior of turbulent swirling flow in an annulus may be examined by using the dimensionless parameter $\tilde{M} = WR$, representing angular momentum, and the dimensionless radial pressure gradient $\partial P/\partial R$. These parameters are plotted for different Ψ and the two initial conditions in Figures 5–8. It may be seen in Figures 5(a) and 5(b) that, in the core region, the

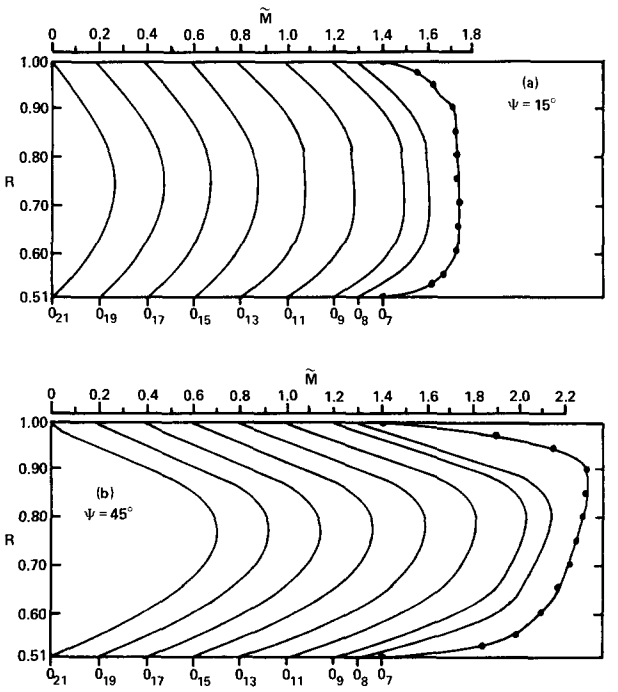

Figure 6 Computed distribution of dimensionless angular momentum in annulus commencing from station 7

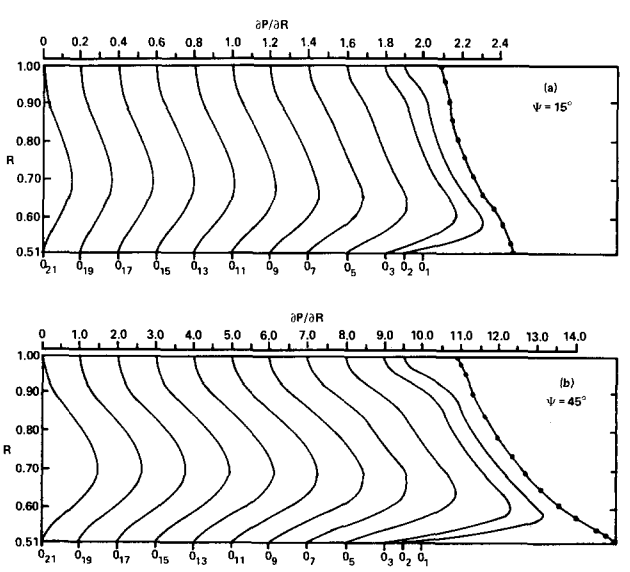

Figure 7 Computed radial pressure gradient in annulus commencing from station 1

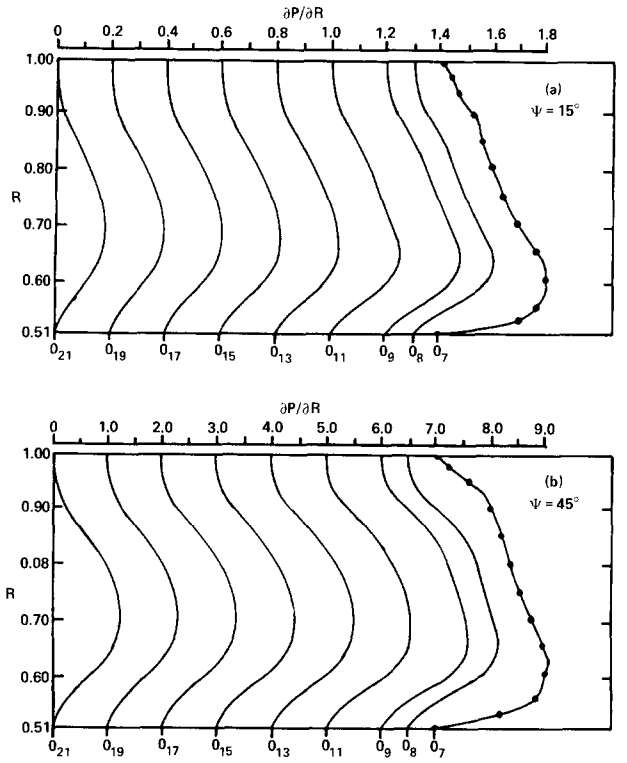

Figure 8 Computed radial pressure gradient in annulus commencing from station 7

variation of $\tilde{M}$ follows that at the entry station 1; indeed, for $\Psi = 15°$, the constancy of $\tilde{M}$ implies free-vortex flow. In each case, the core behavior is maintained approximately to station 8 corresponding to $X = 11.55$; thereafter, the annular variation of $\tilde{M}$ appears approximately parabolic. Near the inner wall $\tilde{M} \propto R^2$, corresponding to forced-vortex flow with the constant of proportionality being a function of the axial position X. However, near the outer wall, $\tilde{M}$ decreases rapidly, implying the possibility of flow instability adjacent to the concave surface. In Figures 6(a) and 6(b), the experimental distributions at station 7 have been used as the starting point for subsequent calculations. We now see the core behavior similar to that at station 7 being extended to station 11 for both values of Ψ, as found from measurements.

The pressure gradient $\partial P/\partial R$ was deduced from Eq. (8). As would be expected, the graphs of Figures 7 and 8 indicate $\partial P/\partial R$ increases as the swirl angle increases. With increasing axial distance downstream, $\partial P/\partial R$ decreases as does $\partial W/\partial R$. In the core region, there is evidently a decrease in $\partial P/\partial R$, with R implying a free-vortex variation of the tangential velocity as discussed earlier. Furthermore, near the outer wall, the pressure gradient is small and, contrary to experimental findings, there is a very small decrease of $\partial P/\partial R$ with R. This anomaly arises from the influence of normal and shear stresses that were neglected in the derivation of the asymptotic solution. One would expect, and indeed we find, a better agreement from the algebraic solution near the inner wall than near the outer wall, as Figure 4 shows.

Figures 9(a)–9(c) show the decay of the local swirl intensity as a proportion of the inlet (maximum) value for different guide vane angles Ψ, radius ratios α and Re. The main characteristics of the flow may be observed; that is, the swirl ratio decreases with X, and for a given X, the ratio decreases slightly as Ψ increases but more significantly as α increases and Re decreases. The data in Figure 9(c) show the swirl decay along the annulus for two values of α and for the free-vortex initial swirl distribution $W = R^{-1}$ used by Scott.[7] Figure 10 plots the swirl decay for the second initial condition, where the initial profile starts at a fully developed station. It can be seen that the swirl decays exponentially with distance downstream and for all the guide vane angles investigated within the first few stations of commencement of the prediction. Thereafter, the decay is virtually linear with slope independent of guide vane angle Ψ, but values of S/S_7 decrease as Ψ increases.

A comparison between the measured[1] tangential profiles and those predicted by this asymptotic theory is shown in Figure 11 for the case $\Psi = 45°$. The theoretical profiles are predicted from the inlet profile of station 1 (at $x = 0$), and it can be seen that significant divergence of results occurs at station 6. Similar behavior was observed for other values of Ψ, α, and Re. This deterioration in the agreement between corresponding profiles continues with distance downstream because boundary-layer growth increases, especially near the outer (concave) wall, and

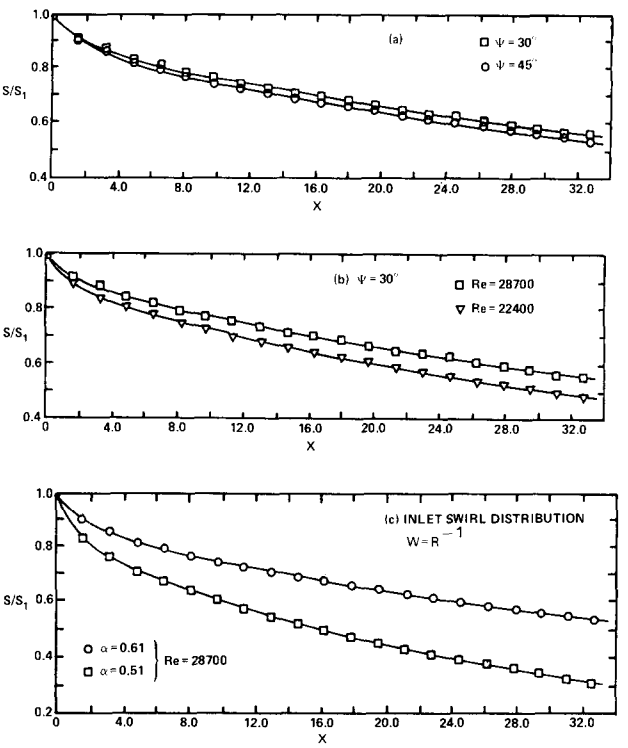

Figure 9 Computed swirl intensities commencing at station 1

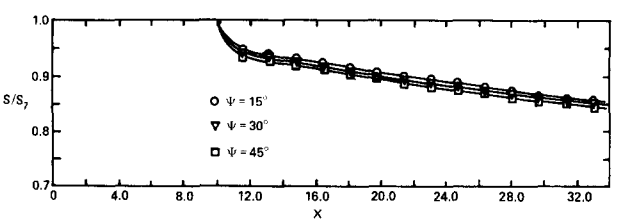

Figure 10 Computed swirl intensities commencing at station 7

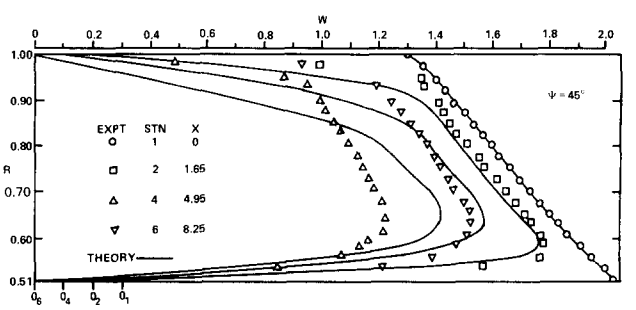

Figure 11 Comparison of computed and experimental dimensionless tangential velocity profiles in annulus commencing from station 1

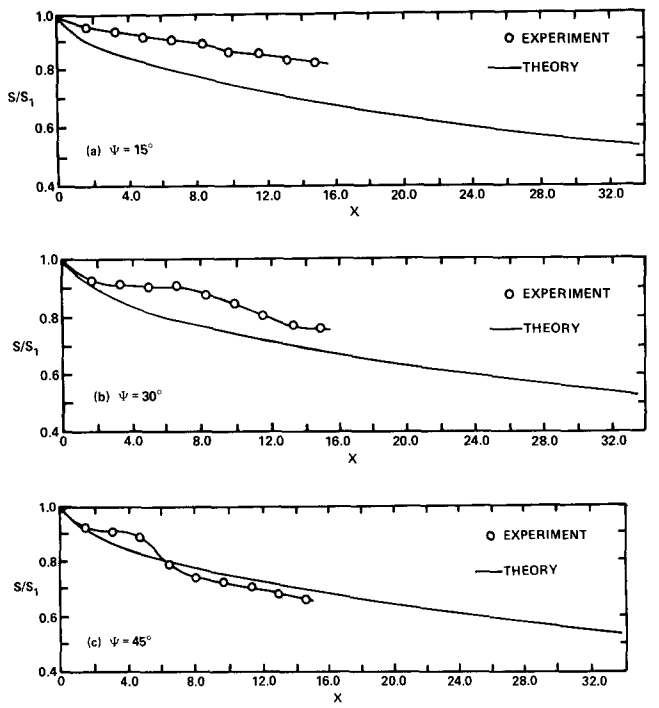

Figure 12 Comparison of computed and experimentally determined swirl intensities in annulus commencing from station 1

applying this technique before the flow is fully developed underpredicts shear stresses in the flow near the outer wall.

Values of the local swirl intensity S, as a proportion of the inlet value S_1 at station 1, have also been calculated from the algebraic solution, again starting at $X=0$. Figures 12(a)–12(c) show data for three values of Ψ, and corresponding experimentally determined variations, within the rig test section, are shown for comparison. With the assumptions used for the algebraic solution it is not, perhaps, surprising that the theoretical curves show little variation with Ψ. More important, there is a large divergence between predicted and measured data, although this difference reduces as Ψ increases from 15° to 45°. Thus although some workers have tried to predict the behavior of swirling flows in an annulus using asymptotic solutions applied from inlet, it can be seen that such an approach is not really satisfactory. The errors involved in applying asymptotic conditions in regions where these do not hold clearly lead to increasing disparity between predicted and measured velocity and swirl distributions with increasing distance along the test section.

Some of our previous work[1] has shown by the time station 7 has been reached, corresponding to $X=9.9$, the flow may be considered fully developed, that is, the U profile has a constant shape. It is, therefore, only for stations beyond this that the asymptotic solution should be used. A comparison between actual and predicted tangential velocity profiles for station 7 and beyond is shown in Figure 13 for $\Psi=45°$, a value that may be considered typical of others. Although the central, virtually linear, part of the curve still defies accurate prediction, there is, nevertheless, sufficiently encouraging agreement between experiment and theory to support the view that a full numerical integration of the equations of motion is needed up to the fully developed flow region, and thereafter, the simpler, asymptotic solution is sufficient. Despite the differences in the actual velocity profiles, integrating these to provide estimates of the swirl intensity shows excellent agreement with similar assessments based on the measured components of flow velocity as shown in Figure 14. Clearly, the discrepancy between the velocity profiles of Figure 13 near the inner and outer walls of the annulus, which arises from the neglect of normal stresses in the asymptotic solution, contributes little to the calculation of swirl intensity.

Conclusions

We have discussed the algebraic, or asymptotic, solution of the equations describing the behavior of swirling turbulent flow passing through an annulus formed between two concentric cylinders of circular cross-section. The theory predicts an exponential decay of swirl along the annulus, which can be represented by $S/S_7=\exp\{-b(X-9{\cdot}9)\}$, where the local swirl parameter S is expressed as a fraction of the value at the start of the fully developed region represented by station 7, where $X=9.9$. The rate of decay of swirl increases with decreasing Reynolds number and with increasing radius ratio α but shows only a slight dependence on the initial swirl angle represented by Ψ. These findings match those reported for the decay of turbulent swirling flow in a circular section pipe.

The profiles of tangential velocity as functions of local radius show that the point at which W is a maximum moves out radially toward the concave wall as development takes place from the inlet profile that has a near free-vortex nature. Nevertheless, even at the last station in the test section, the maximum W point is still nearer to the convex wall than the concave wall, which supports the results of other workers dealing with less rigorous theories and experimental procedures.

An examination of theoretical and experimental data has shown that, at least for our investigations, the eddy kinematic viscosity can be expressed as a function of only Re and has the form

$$\varepsilon=0.404\nu(\mathrm{Re})^{0.305}$$

We have shown that the algebraic (asymptotic) solution to the equations of motion can produce acceptable results if applied correctly. That is, the calculations should commence at a location in the annulus where fully developed flow exists. If, as some workers have done, the method of solution is allowed to commence at the annulus inlet, substantial errors are incurred.

In a series of papers, we have presented and analyzed experimental results from annulus flows and developed several theoretical approaches. The numerical integration of equations developed from the Navier-Stokes equations has been shown to give good predictions but at the expense of large computing

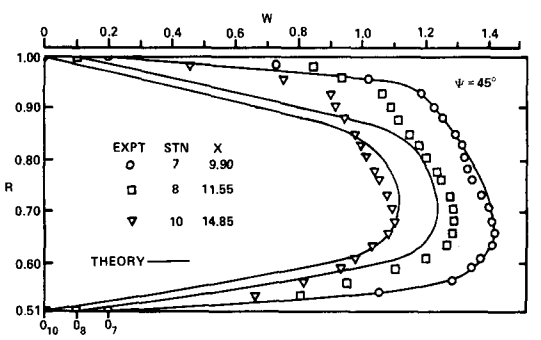

Figure 13 Comparison of computed and experimental dimensionless tangential velocity profiles in annulus commencing from station 7

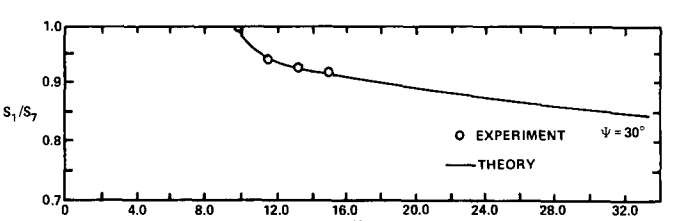

Figure 14 Comparison of computed and experimentally determined swirl intensities in annulus commencing from station 7

times and storage. However, the use of the techniques discussed in this paper results in the restriction of the numerical technique to the point at which the flow is considered fully developed; thereafter, a simpler analysis can be used with good accuracy. Finally, it may be concluded that all theoretical approaches require adopting some kind of turbulence model, and as yet, no sufficiently accurate general form is available. More work is evidently required on that particular topic before an entirely theoretical prediction can be developed and used for a broad class of swirling flows.

References

1 Clayton, B. R. and Morsi, Y. S. M. Determination of principal characteristics of turbulent swirling flow along annuli. part 1: measurement of time mean parameters. *Int. J. Heat and Fluid Flow*, 1984, **5**(4), 195–203

2 Clayton, B. R. and Morsi, Y. S. M. Determination of principal characteristics of turbulent swirling flow along annuli. part 2: measurement of turbulence components. *Int. J. Heat and Fluid Flow*, 1985, **6**(1), 31–41

3 Morsi, Y. S. M. and Clayton, B. R. Determination of principal characteristics of turbulent swirling flow along annuli. part 3: numerical analysis. *Int. J. Heat and Fluid Flow*, 1986, **7**, 208–222

4 Talbot, L. Laminar swirling pipe flow. *J. Appl. Mech. Trans. ASME.*, 1954, **21**(76), 1–7

5 Wolf, J. R., Lavan, Z. and Fejer, A. A. Measurements of the decay of swirl in turbulent flow. *AIAAJ*, 1969, **7**, 861–973

6 Kiya, M., Fukusako S, and Arie, M. Laminar swirling flow in the entrance region of a circular pipe. *Bull. JSME*, 1971, **14**, 659–670

7 Scott, C. J. A series solution for decay of swirl in an annulus. *J. Appl. Mech., Trans. ASME*, 1972, **39**(94), 289–290

8 Kreith, F. and Sonju, O. K. The decay of turbulent swirling flow in a pipe. *J. Fluid Mech.*, 1965, **22**, 257–271

9 Rochino, A. and Lavan, Z. Analytical investigations of incompressible turbulent swirling flow in stationary ducts. *J. Appl. Mech., Trans. ASME*, 1969, **36**(91), 151–158

10 Yeh, H. Boundary layer along annular walls in a swirling flow. *Trans. ASME*, 1958, **80**, 767–776

11 Morsi, Y. S. M. Analysis of turbulent swirling flows in axisymmetric annuli. PhD thesis, University of London, 1983

12 Wylie, C. R. *Advanced Engineering Mathematics*, 3d ed, McGraw-Hill, New York, 1966

13 Bragg, S. L. and Hawthorne, W. R. Some exact solutions of the flow through annular cascade actuator discs. *J. Aeronaut. Sci.*, 1950, **17**, 243–249

14 Hawthorne, W. R. and Horlock, J. H. Actuator disc theory of the incompressible flow in axial compressors. *Proc. Instn. Mech. Engrs.*, 1962, **176**(30), 789–812